



## A NEW TYPE OF TRI-AXIAL ACCELEROMETERS WITH HIGH DYNAMIC RANGE MEMS USING FOR EARTHQUAKE EARLY WARNING

C.Y. Peng<sup>(1)</sup>, J.S. Yang<sup>(2)</sup>, X.Y. Zhu<sup>(3)</sup>, Y. Chen<sup>(4)</sup>, Q.S. Chen<sup>(5)</sup>, H.T. Wang<sup>(6)</sup>

<sup>(1)</sup> Associate Professor, Institute of Geophysics, China Earthquake Administration, Beijing, 100081, China, [pengchaoyong@cea-igp.ac.cn](mailto:pengchaoyong@cea-igp.ac.cn)

<sup>(2)</sup> Professor, Institute of Geophysics, China Earthquake Administration, Beijing, 100081, China, [yangjs@cea-igp.ac.cn](mailto:yangjs@cea-igp.ac.cn)

<sup>(3)</sup> Senior Engineer, Institute of Earthquake Science, China Earthquake Administration, Beijing, 100036, China, [zhuxy@geodevice.cn](mailto:zhuxy@geodevice.cn)

<sup>(4)</sup> Senior Engineer, Institute of Earthquake Science, China Earthquake Administration, Beijing, 100036, China, [bicheny@263.net](mailto:bicheny@263.net)

<sup>(5)</sup> Hardware Engineer, Beijing Gangzhen Instrument & Equipment Co., LTD, Beijing, 102628, China, [chenqs@geodevice.cn](mailto:chenqs@geodevice.cn)

<sup>(6)</sup> Professor, Institute of Earthquake Science, China Earthquake Administration, Beijing, 100036, China, [wanght@geodevice.cn](mailto:wanght@geodevice.cn)

### Abstract

Earthquake Early Warning System (EEWS) has been proved to be one of the effective ways for earthquake damage mitigation. As the progress of low-cost Micro Electro Mechanical System (MEMS), many types of MEMS-based accelerometers have been developed and widely used in deploying large-scale, dense seismic networks for EEWS. However, the noise performance of these commercially available MEMS is still insufficient for weak seismic signals, leading to the large scatter of early-warning parameters estimation. In this study, we developed a new type of tri-axial accelerometer based on high dynamic range MEMS with low noise level using for EEWS. It is a MEMS-integrated data logger with built-in seismological processing. The device is built on Linux 2.6.27 operating system and STA/LTA algorithm is used to automatically detect seismic events. When a seismic event is detected, peak ground parameters of all data components will be calculated at an interval of 1 s, and  $\tau_c$ - $P_d$  values will be evaluated using the initial 3 s of P wave. These values will then be organized as a trigger packet actively sent to the processing center for event combining detection. The output data of all three components are calibrated to sensitivity 500 counts/cm/s<sup>2</sup>. Several tests were performed to obtain the performances of this device. The results show that the dynamic range can reach 98 dB for the vertical component and 99 dB for the horizontal components, and majority of bias temperature coefficients are lower than 200  $\mu\text{g}/^\circ\text{C}$ . In addition, the results of STA/LTA event detection have shown its capabilities for EEWS and rapid intensity reporting.

*Keywords: earthquake early warning; MEMS-based accelerometer; high dynamic range; STA-LTA event detection; low-latency data packet*



## 1. Introduction

With the development of the global economy, rapid urbanization makes modern societies more vulnerable to natural disasters, especially for areas with populations exceeding 10 million like Beijing, Shanghai. Therefore, it is very important to build early warning systems as one means of mitigating damage induced by such disasters. Considering earthquakes, many areas of major urbanization (e.g., Tokyo, Istanbul, Naples, Mexico City) are exposed to significant seismic hazard. Currently, several parts of the world have already developed earthquake early warning system (EWS), or are on the verge of doing so [1-19].

EWS are typically classified as either regional or on-site early warning systems. For the regional one, it is based on the use of a seismic network located near the expected epicentral area, with the aim of detecting, locating, and determining the size of an earthquake in terms of classes considering recorded ground motions, or directly estimating the magnitude, all based on the analysis of the first few seconds of the initial P-waves. This information is then used in appropriate ground motion prediction equations to estimate the shaking at a specific site, with the warning sent by modern communications means, hence exploiting the much faster speed of electromagnetic signals over seismic waves. Such systems are the optimal solution when the seismogenic area is well known and rather far from the site to protect. By contrast, for target sites too close to a seismogenic area, the on-site early warning systems, which are based on the idea of using seismic sensors directly at the target site, are preferable. Again, by exploiting information carried by the faster P-waves, the size of the larger shaking associated with the incoming S and surface waves may be inferred.

Generally, these systems usually involve the use of a relatively low number of sensors, a fact largely dictated by the high cost of such instrumentation. Although in some regions such as Japan, Taiwan, the station density of their seismic networks is proven to be rather adequate for rapid reporting and earthquake early warning (EEW) purposes [20], a higher density of seismic stations is always in great demand [21,22] especially for a front-detection type of EWS, in which the seismograms recorded by closer-to-earthquake seismic sensors are used to estimate the earthquake location, magnitude, and to predict the ground motions at more distant target areas. For example, a short-distance EWS might be possible with extensive installation of seismometers around seismogenic areas [23]. However, to increase the number of seismic station equipped with traditional mechanical seismometer will significantly boost the expense of EEW seismic network. Besides, for the other seismogenic zones around the world where only a limited number of seismic stations or even no seismic network is available, a cost-effective seismic network dedicated to EEW or rapid reporting is highly favored.

Micro-Electro Mechanical System (MEMS) accelerometers have been introduced in seismic applications since 1990s [24]. It is a miniature device which can provide a cost-saving, ideal solution for recording unsaturated, near-field, and high-frequency ground-motion signals. Therefore, this type of accelerometers offers a suitable application to developing an economical, large-scale seismic networks with high density. The MEMS accelerometer type of network has been proved to be potential for EEW using the Quake-Catcher [25] and Palert network [26].

Recently we have developed an integrated onsite EWS called EDAS-MAS [27] which can issue warning through sound, LCD display and SMS to the local site when the estimated early-warning parameters exceed the preset thresholds. With 7 months of test deployment, the results have shown that this onsite EWS can obtain robust estimation of  $M_{pd}$  using the  $P_d$  attenuation relationship proposed by [28,29]. However, for the  $\tau_c$  early-warning parameter, the results have huge scatter, and many of them are unreasonably large. This is due to the low signal-to-noise ratio (SNR) of the recorded acceleration waves because the accelerometer used in the system is a type of Class-C MEMS-based sensors with low useful resolution [30]. In addition, in the test period, we found that some functions designed in the system are useless, such as LCD display, touch screen. Moreover, few functions like 3G/GSM, wireless fidelity and sound card can be removed from the system and carried out with other independent devices.

Therefore, for improving the SNR of the acceleration records and reducing the complexity of the device, in this work, we designed a new type of tri-axial accelerometers called GL-P2B with high dynamic range MEMS using for EEW. It is a MEMS-integrated data logger with built-in seismological processing, including low-latency data packet transfer, and early-warning parameters calculation. This device is built on a customized



Linux 2.6.27 operating system and STA/LTA algorithm is adopted to automatically pick the P-wave arrival. Many useless functions existed in EDAS-MAS are removed from this instrument.

## 2. Design and implementation

The appearance and a block diagram of GL-P2B are shown in Fig. 1. Its hardware structure can be divided into five parts: three single-component MEMS-based accelerometers, three analog-to-digital converter (ADC) modules, a field programmable gate array (FPGA), an ARM CPU and some peripheral components such as 64 MB NAND Flash, 8 GB CF card, 64 MB SDRAM, 10/100M Ethernet. Signals from ground-motion are firstly picked by the three MEMS-based accelerometers and converted into digital signals through ADC. They will be organized into specified formats in FPGA and transferred to the ARM CPU by the serial synchronous controller (SSC). Then the CPU will use minimum-phase FIR filters to process these data and store them into a big ring buffer in the Linux kernel. Applications can read data from kernel through the Linux device interface and use them for storing, estimating seismic parameters, transferring, etc. All components are brought off-the-shelf, leading to GL-P2B being much less expensive (about 6000 RMB or US\$1000 per unit) than traditional strong-motion accelerometers.

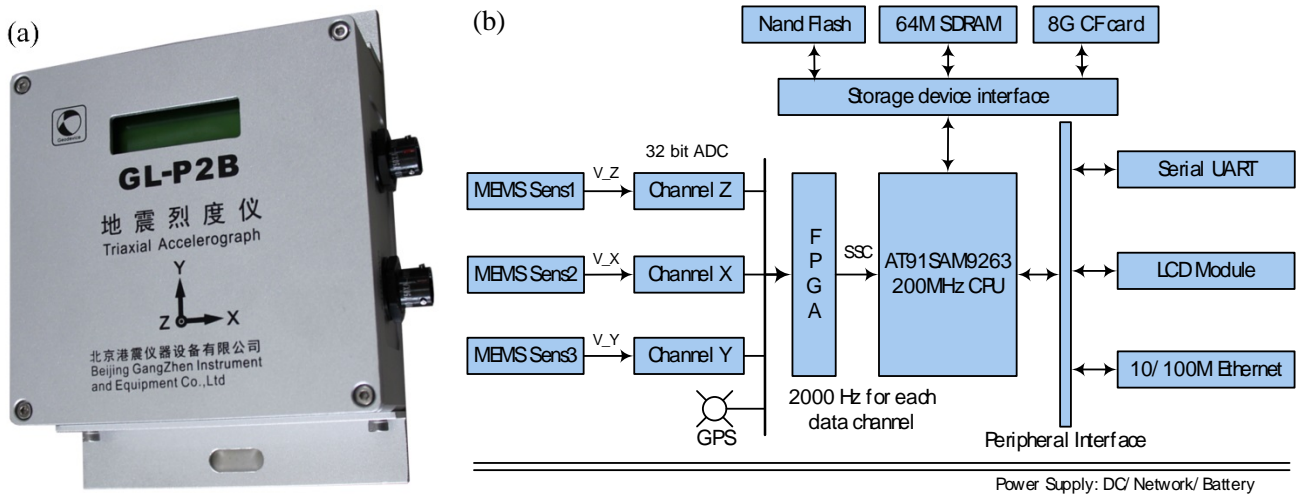


Fig. 1 – The appearance and a block diagram of GL-P2B. (b) is modified from [27].

### 2.1 Hardware implementation

Two custom designed PCB boards have been fabricated to contain all hardware components except the sensor. One is called AD board, and the other one is the power board including the ARM CPU. The device dimension is 150 mm (length) \* 150 mm (width) \* 68 mm (height), and its weight is ~ 1.98 kg.

To the sensor, we have arranged three independent MEMS-based accelerometers to provide three component (Z, X, and Y) data. The MEMS sensor is a custom designed version derived from MSV6000 variable capacitance accelerometers [31] which can provide a selectable full-scale of  $\pm 2/10/30/50/100/200/500/1000/10000/20000$  g with relevant sensitivities ( $1000\pm 8, 200\pm 2, 66.6\pm 1, 40\pm 1, 20\pm 1, 10\pm 1, 4\pm 0.3, 2\pm 0.3, 0.2\pm 0.03, \text{ and } 0.1\pm 0.01$  mV/g) and resolutions (0.002, 0.01, 0.05, 0.1, 5, 7.5, 15, 20, 200, and 400 mg@1Hz). Generally, the full-scale of 10 g or more is not suitable for seismic recording, because we usually need relatively high resolution for weak motions. Therefore,  $\pm 2$  g is selected for GL-P2B, then its bandwidth ( $\pm 5\%$ ), sensitivity, noise density, bias temperature coefficient, and resolutions are DC-250 Hz,  $1000\pm 8$  mV/g,  $10 \mu\text{V}/\sqrt{\text{Hz}}$ , less than  $0.2 \text{ mg}/^\circ\text{C}$ , and  $0.002 \text{ mg}/1\text{Hz}$ , respectively.

For the ADC modules, the ADS1281 [32] which is an extremely high-performance, single-chip ADC designed for the demanding needs of energy exploration and seismic monitoring environments is chosen for data acquisition and conversion. It contains a fourth-order, inherently stable, delta-sigma modulator and a digital filter



including a sinc and finite impulse response (FIR) low-pass stages followed by an infinite impulse response (IIR) high-pass filter stage. The sampling rate we used here is 2000 samples per second (SPS).

A3P250 is selected as the FPGA, which is one of the third-generation family of Microsemi flash FPGAs (ProASIC3) [33] offering 1 kbit of on-chip, reprogrammable, nonvolatile FlashROM storage as well as clock conditioning circuitry based on an integrated phase-locked loop (PLL). A data format regulation is defined for FPGA to code data from ADC and GPS. These coded data will be transferred to the CPU through SSC.

GL-P2B uses the same ARM processor as EDAS-MAS [27]. However, the CPU frequency is reduced to 200 MHz for power saving. The Linux 2.6.27 operating system (OS) with 2.6.27-at91 patch is run on the CPU. The storage device includes a 8GB+ CF card acting as the hard disk, and a 64 MB NAND Flash for storing the YAFFS file system compiled within Busybox 1.0.6.

## 2.2 Software functions

The software designed for GL-P2B currently includes the following, except the seismological processing. Here we only describe software functions different from those designed in EDAS-MAS [27].

- **Linux OS:** The OS for GL-P2B is a custom-tailored Linux 2.6.27 with 2.6.27-at91 patch. Only device drivers for SCSI ports, MTDBLOCK, FLASH, LCD, and network are remained. YAFFS is selected as the file system, and NFS is used for the BusyBox burned. We have added some new character device drivers to the system for real-time data filtering & buffering, system parameter managing, temperature measurement, WatchDog, and power management. The configured Linux kernel codes are compiled by the ARM Cross Compiler 3.4.2. For system startup, the U-Boot is used to initialize hardware, to uncompress and load the Linux kernel, and to hand over control to Linux. It is stored in the initial address of the flash memory. After the Linux kernel startup is complete, the system will enter into the BusyBox environment through User/Password input. The BusyBox implements many Linux system commands, such as ls, cd, ftp and telnet. All these together form the custom-tailored Linux OS, and 15 MB NAND Flash storage is reserved to keep it.

- **Sensitivity adjustment:** Due to the integrated design of hardware structure, sensitivity of each device is uniformly adjusted to 500 counts/cm/s<sup>2</sup>. A configuration file 'zero\_offset' saved under directory '/usr/conf/' is used to set sensitivity adjustment parameters of the three data components after box-flip tests [34], which can obtain the static sensitivity, offset, and orientations of every axis. Each component of data will be multiplied by its sensitivity adjustment parameter and rounded to integer before recording to the CF card or transferring to the processing center.

- **Real-time data service:** The real-time data transmission mode (TM) is set by the transmission mode control packet (TMCP) returned from the processing center, namely server. Three different data transmission modes are supported in GL-P2B:

- 1) **Continuous wave TM:** The continuous waveform encoded in MiniSEED format is transferred to server immediately after the connection between GL-P2B and server is built. The server will not respond to each data packet until GL-P2B receives a different TMCP. In this mode, GL-P2B will not detect triggering information and send "heartbeat" message to the server.

- 2) **Waveform TM when an event is triggering:** The "heartbeat" message is sent to the server at an interval of 10 s after the network connection between GL-P2B and server is built. When an event is triggering, waveform and triggering information will be simultaneously sent to the server until the event is end. Here the waveform data includes 30 s cached data before the trigger and current real-time data. If the event is end, GL-P2B will convert to send the 10 s interval "heartbeat" message.

- 3) **Non-waveform TM when an event is triggering:** This mode is similar to the previous one. The difference is that, when an event is triggering, only triggering information is sent to the server at an interval of 1 s until the event is end. In addition, in the period of event triggering, the "heartbeat" message will be continuously sent to the server.

- Time service: GPS and NTP are combined to adjust the local clock and provide system time service for GL-P2B. The time accuracies when the local clock is synchronized against GPS and NTP are 10  $\mu$ s and 2 ms, respectively. The detailed information can be found in [35].
- LCD display: Five types of system status information are set to the LCD screen as a loop display at an interval of 2 s. These statuses include (a) Vendor and device names, (b) current data and time, (c) IP address and serial baud-rate, (d) storage status of CF card, and (e) timing information.

### 2.3 Seismological processing

The primary goal of developing GL-P2B is to perform real-time seismological analysis of rapid intensity reporting and EEW. Therefore, we mainly focus on the real-time seismological data processing, including data filtering, low-latency data organizing, automatic seismic event detecting, ground-motion parameters calculating and transferring.

For data filtering, the 2000 Hz real-time data received from the FPGA through SSC is firstly extracted and filtered by a FIR 71th order low-pass filter with minimum phase into a sample of 400 Hz, and then extracted and filtered by a similar FIR filter with 135th order coefficients into a sample of 200 Hz. Data of 100 Hz and 50 Hz are processed with the same filter and extracted from 200 Hz and 100 Hz, respectively. To reduce the CPU load, we use ARM assembly language to code the FIR filtering algorithms. In addition, we also adopt methods of loop unrolling and caching multiple data for filtering at each processing time.

As for low-latency data organizing, we put the filtered real-time data into ring buffers with time-index pointer lists. For each channel, sampling rate and phase type, there are a real-time data buffer and a corresponding time-index pointer list which can cache data of 40 s. When a user starts fetching real-time data, he firstly needs to set sampling rate, phase type and data frame length (*fra\_len*). The application will first locate position of the latest second (*newest\_sec*) according to the sampling rate and phase type. Then real-time data will be fetched with the length defined by *fra\_len*. If the data length between last acquired data position (*last\_pos*) and the latest data point (*newest\_data*) is bigger than *fra\_len*, the real-time data will be continuously fetched and *last\_pos* will be updated as *last\_pos* plus *fra\_len* until the length of the rest data is smaller than *fra\_len*. This will ensure that length of the delayed points is less than *fra\_len*. If *fra\_len* and sampling rate are set as 20 and 200 Hz, the real-time data latency will be 0.1 s.

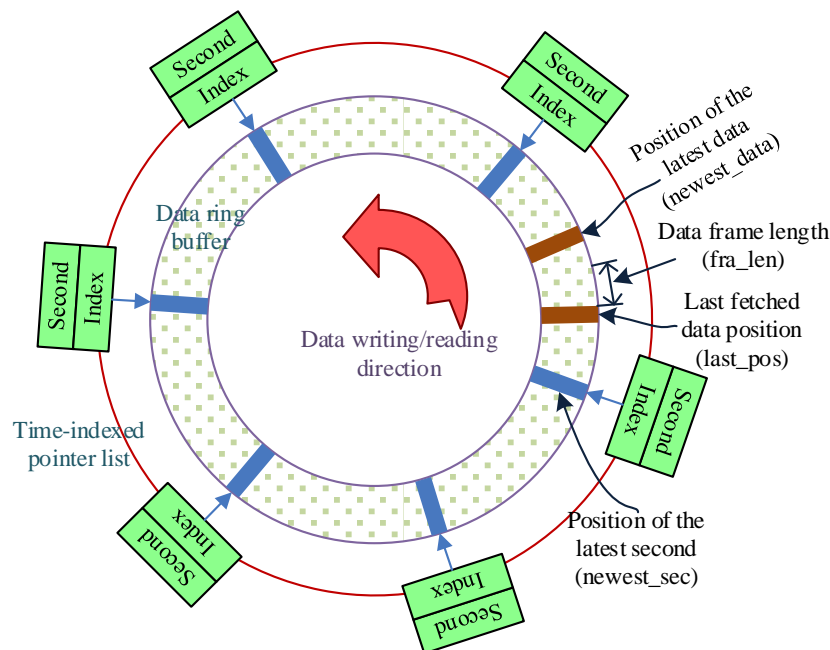


Fig. 2 – Low-latency data organization and access mode



Automatic seismic event detecting is one of the most basic seismological processing steps. Using an appropriate automatic detection algorithm can ensure the correctness of earthquake event recordings and reduce the follow-up data processing workload of digital earthquake observation. In principle, triggering can be performed using any real-time algorithm, under the constraint that it cannot be done with any method that requires data after the trigger itself, because by definition such data is unavailable at the time of the trigger [11]. Therefore, methods such as autoregressive pickers [36] and pickers based on wavelet transforms [37], are not practically suitable for early warning applications even though they are more precise than a simple short-term/long-term average (STA/LTA) algorithm [38-41]. For this reason, we adopt STA/LTA that is a classical seismic event detection algorithm in GL-P2B. Its basic principle is to process filtered seismic signals in two moving time windows: A short-time average window (STA) and a long-time average window (LTA). The STA is used for measuring the instant amplitude of the seismic signal and watching for earthquakes. The LTA is used to deal with the current average seismic noise amplitude. The accelerometer data will be filtered using a 4<sup>th</sup> order bandpass (0.1 – 10 Hz) Butterworth filter before the STA/LTA detection. When the SNR for P waves of UD component exceeds a predefined value, the system is triggered. We use the recursive formulation proposed by NORSAR [39,40], where the SNR for P waves is updated at every data point. In order to make sure that the P- and not S-wave is picked, an event end threshold is set as 1.3 times of the LTA value which is frozen at the moment of the P-wave trigger. If the STA values is bigger than this value, we believe that the event is still in progress. Otherwise, the event is end.

Immediately after triggering, peak ground parameters of all data components are computed from the filtered acceleration records at an interval of 1 s until the end of the event. These parameters include peak ground acceleration (*PGA*), peak ground velocity (*PGV*), peak ground displacement (*PGD*), instrumental seismic intensity, spectral acceleration at 0.3 s period (*PSA03*), spectral acceleration at 1.0 s period (*PSA10*) and spectral acceleration at 3.0 s period (*PSA30*). In addition, the early-warning parameters,  $\tau_c$  and  $P_d$ , will also be calculated from the 3-s vertical component waveform after *P*-wave arrival. At every second, these results will be organized as a trigger packet and actively sent to the processing center for combining detection. The format of the trigger packet is defined in ‘provisional technical requirements of data transmission protocol for seismic intensity instrument (in Chinese)’.

### 3. Performance tests

For obtaining the performance of this device, we performed several main tests on it, including dynamic range tests, bias temperature coefficient tests, amplitude-frequency characteristics tests, and event triggering tests.

#### 3.1 Dynamic range (DR) tests

DR is determined from the largest and smallest signals that can be recorded by the instrument [42-45]. Here, the largest signals, also called clip levels, is set as 2 g. The smallest signals, also called instrument self-noise, are generally obtained from recorded records, when the sensors are fixed to a low-noise pier during a late-night interval with low cultural and wind noise. However, for this device, because the sensor noise is well above the site noise, we attribute all of the sensor output to instrument noise. To obtain the instrument self-noise, we selected a test site with acceleration noise spectral density smaller than  $5 \cdot 10^{-7} \text{ m}/(\text{s}^2 \cdot \sqrt{\text{Hz}})$  in the frequency band of 0.01 to 50 Hz. Firstly, we installed the instruments onto the test site, and set them to record data at a sampling rate of 100 Hz. The recording time is greater than 10 minutes. We then selected 300 s length data with no significant interference from the original records, and a bandpass (0.1 – 20 Hz) Butterworth filter with octave attenuation bigger than 12 dB was used to filter these data. The root mean square of the filtered data was finally set as the instrument self-noise. The DR can be computed from

$$\text{DR} = 20 \lg \frac{0.707A}{N}, \quad (1)$$

where  $A$  is the clip level, and  $N$  is the instrumental self-noise. The test results are shown in Fig. 3 and Table 1.

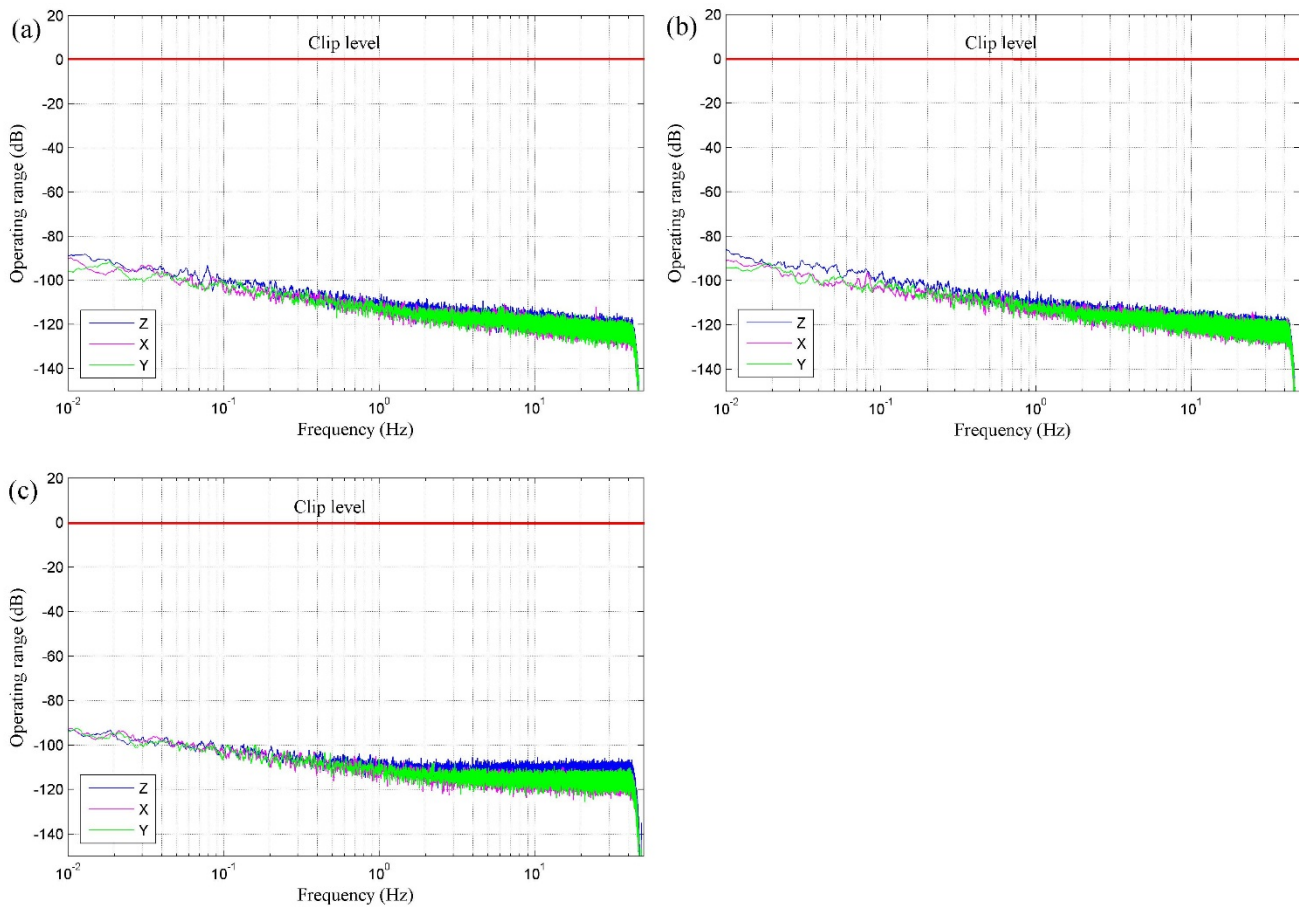


Fig. 3 – Dynamic range of three GL-P2B: (a) Sensor A, (b) Sensor B, and (c) Sensor C.

Table 1 – Dynamic range of three GL-P2B

No.	Z (UD)	X (EW)	Y (NS)
Sensor A	97.46	97.85	97.19
Sensor B	98.35	98.25	99.13
Sensor C	98.17	97.27	99.09

### 3.2 Bias temperature coefficient (BTC) test

To acquire the bias temperature coefficient of these three GL-P2B, a temperature control system is used. Different temperature was set, and at each temperature the devices at least record four-hours data. We totally spend more than two days on the test. The results can be found in Table 2 and Fig. 4.

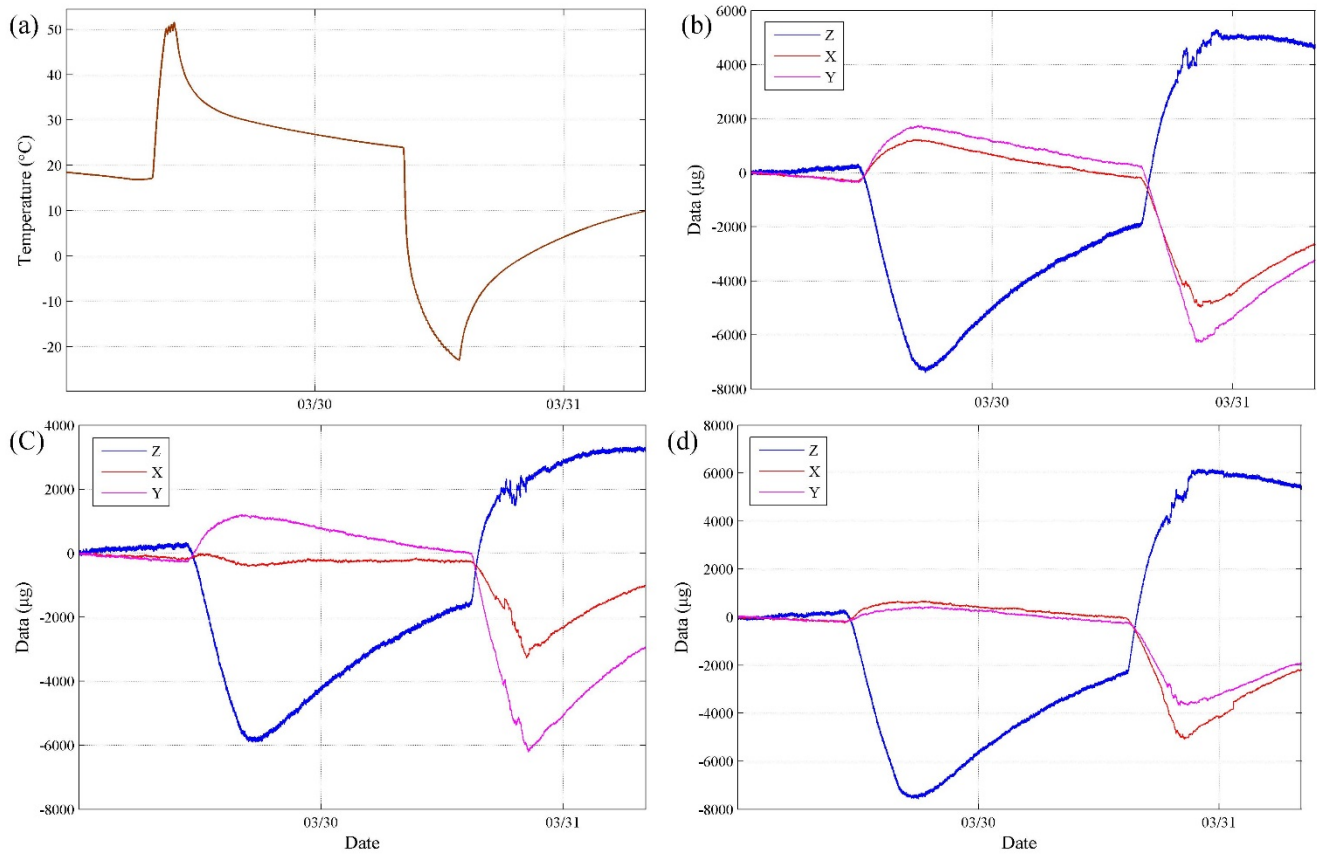


Fig. 4 – Bias temperature coefficient test results of three GL-P2B. (a) Temperature curve; (b)(c)(d) are data varying with temperature recorded by sensor A, B, and C, respectively.

Table 2 – BTC test results of three GL-P2B

No.	BTC ( $\mu\text{g}/^\circ\text{C}$ )			Data variation range ( $\mu\text{g}$ )		
	Z (UD)	X (EW)	Y (NS)	Z (UD)	X (EW)	Y (NS)
Sensor A	215.54	-88.41	-115.74	12697.11	6211.86	8011.87
Sensor B	159.04	-28.80	-103.09	9248.91	3583.88	7420.71
Sensor C	242.53	-75.97	-57.18	13754.79	5773.43	4127.56

### 3.3 Amplitude-frequency characteristics test

We measured amplitude-frequency characteristics using a linear shake table with operating frequency range of 0.0002-200 Hz, maximum displacement of 20 cm, maximum acceleration of  $10 \text{ m/s}^2$  and maximum load of 30 kg to input sine-wave motion at various amplitudes and frequencies, and comparing the output signals recorded at a sample rate of 200 Hz with these input reference signals. In this test, we did not use an independent reference sensor for the shake table. Therefore, we generated synthetic sine waves of the known input amplitude and frequency, but no phase information, and calculated amplitude ratios relative to this synthetic sine wave. The results of the three GL-P2B are listed in Table 3.



Table 3 – Amplitude-frequency characteristics test results of three GL-P2B

Freq. (Hz)	Sensor A			Sensor B			Sensor C		
	Z (UD)	X (EW)	Y (NS)	Z (UD)	X (EW)	Y (NS)	Z (UD)	X (EW)	Y (NS)
1	1.0108	0.9945	0.9943	1.0106	0.9947	0.9930	1.0065	0.9928	0.9936
5	1.0117	0.9947	0.9946	1.0134	0.9951	0.9943	1.0095	0.9955	0.9950
10	1.0125	0.9963	0.9957	1.0423	0.9966	0.9954	1.0121	0.9952	0.9961
20	1.0110	0.9961	0.9960	1.0151	0.9971	0.9956	1.0113	0.9956	0.9958
30	1.0123	0.9986	0.9988	1.0132	1.0004	0.9983	1.0090	0.9988	0.9984
40	1.0126	0.9996	1.0001	1.0135	1.0024	0.9993	1.0128	1.0002	0.9987
60	1.0062	1.0044	1.0059	1.0096	1.0106	1.0038	1.0081	1.0072	1.0020
78	1.0047	1.0041	1.0074	1.0054	1.0023	1.0047	1.0049	1.0046	1.0069

### 3.4 Event triggering test

For testing the automatic event triggering performance of GL-P2B, a sledgehammer was used to strike the ground adjacent to an installed GL-P2B. We tested it with three times. Only the results of Z component are listed in Table 4. In order to check correctness of the automatic output results, we manually calculate the same parameters from a waveform file downloaded from the CF card in GL-P2B through FTP, also listed in Table 4.

Table 4 – Event triggering results of Z component

No.	Triggering period	Remark	P-wave arrival time (hh:mm:ss.ss)	Instrumental seismic intensity	PGA (cm/s <sup>2</sup> )	PGV (cm/s)	PGD (cm)
1 <sup>st</sup>	20:04:51-20:05:29	Automatic output results	20:04:50.19	5.3	66.70	1.90	3.94
		Manually calculated results	20:04:50.14	5.1	52.17	2.03	0.84
2 <sup>nd</sup>	20:09:01-20:09:41	Automatic output results	20:09:02.47	5.5	70.60	2.60	3.37
		Manually calculated results	20:09:02.42	5.3	54.97	1.89	1.01
3 <sup>rd</sup>	20:09:50-20:10:36	Automatic output results	20:09:50.85	6.3	130.90	4.30	6.71
		Manually calculated results	20:09:50.78	6.2	110.07	4.57	1.40

## 4. Discussion and conclusion

Nowadays, many MEMS-based accelerometers have been developed for EEW. However, because these sensors are a type of Class-C sensors with low useful resolution and low SNR, waveform recorded by them cannot be used for calculating the frequency-based early-warning parameters like  $\tau_c$  and  $\tau_p^{max}$ . For improving the quality of the recorded acceleration waves, in this study, a new type of tri-axial accelerometers called GL-P2B with high dynamic range MEMS has been developed. It is a MEMS-integrated data logger with built-in seismological processing, including low-latency data packet transmission, automatic P-wave arrival detection, and early-warning parameters calculation. Some useless functions existed in EDAS-MAS, an integrated onsite EEWs



recently developed by us, are removed from this new device, such as LCD display, touch screen, 3G/GSM, wireless fidelity and sound card. This leads to the power of GL-P2B much lower than that of EDAS-MAS (2 W vs. 5-8 W at 5 V DC).

After the completion of system development, we performed many tests on the device for obtaining its performances, including DR tests, BTC tests, amplitude-frequency characteristics tests, and event triggering tests.

From the results of DR tests, as shown in Table 1 and Fig. 3, the DR of each component of GL-P2B is bigger than 97 dB, and some can reach 99 dB. That is to say, the equivalent bits resolution (peak only) of the device can reach 17 useful bits (18 bits peak-to-peak), which is comparable to GeoSIG model GMS-18, one type of Class B sensor with an effectively 16-bit (vertical) and 18-bit (horizontal) instrument [34]. As to the BTC, one can find that the BTC of the Z (UD) component is generally bigger than those of the horizontal components, and majority of BTCs of horizontal components are lower than 100  $\mu\text{g}/^\circ\text{C}$ . This performance is better than many traditional strong-motion accelerometers like Guralp CMG-5TC, Namometrics Titan, RefTek RT-147-01/3, and can be compared with EpiSensor 2, the world's first seismological-grade strong-motion accelerometer [46]. For the amplitude-frequency characteristics, the test results listed in Table 3 show that GL-P2B exhibits a nearly flat to about 80% of the Nyquist frequency. This pattern is in general conformity with Class-A and Class-B accelerometers though the sharpness and phase of the high-frequency corner rolloff varies, most often in a manner controlled by the delta-sigma ADC decimation filtering.

For checking the correctness of P-wave arrival time and ground-motion parameters, we use a sledgehammer to strike the ground adjacent to an installed GL-P2B and compare the automatic output results with the manually calculated ones. From the results listed in Table 4, we can find that the P-wave arrival time, instrumental seismic intensity, PGA, and PGV are almost the same as each other. However, when referred to PGD, there is a huge difference between these two results. The reason may be due to the operation caused by the double integration for obtaining displacement values.

In all, these test results suggest that GL-P2B can be classified as a type of Class-B sensor, and it is an acceptable device for EEW and rapid intensity reporting.

## Acknowledgements

We are grateful to Beijing Gangzhen Instrument & Equipment Co., LTD for providing hardware environment and a shake table to develop and test the device. The development and implementation of the system described in this study has been partially co-funded by Basic Research Project of Institute of Geophysics, China Earthquake Administration (DQJB15C04, DQJB14B05) and the National Natural Science Foundation of China (41404048).

## References

- [1] Wu YM, Teng TL (2002): A virtual sub-network approach to earthquake early warning. *Bulletin of the Seismological Society of America*, **92**, 2008-2018.
- [2] Wu YM, Zhao L (2006): Magnitude estimation using the first three seconds P-wave amplitude in earthquake early warning. *Geophysical Research Letters*, **33**, L16312.
- [3] Chen DY, Hsiao NC, Wu YM (2015): The earthworm based earthquake alarm reporting system in Taiwan. *Bulletin of the Seismological Society of America*, **105**, 568-579.
- [4] Horiuchi S, Negishi H, Abe K, Kamimura A, Fujinawa Y (2005): An automatic processing system for broadcasting system earthquake alarms. *Bulletin of the Seismological Society of America*, **95**, 347-353.
- [5] Hoshiba M, Kamigaichi O, Saito M, Tsukada S, Hamada N (2008): Earthquake early warning starts nationwide in Japan. *Eos, Transactions American Geophysical Union*, **89** (8), 73-74.
- [6] Allen RM, Kanamori H (2003): The potential for earthquake early warning in southern California. *Science*, **300**, 786-789.



- [7] Böse M, Ionescu C, Wenzel F (2007): Earthquake early warning for Bucharest, Romania: Novel and revised scaling relations. *Geophysical Research Letters*, **34**, L07302.
- [8] Alcik H, Ozel O, Apaydin N, Erdik M (2009): A study on warning algorithms for Istanbul earthquake early warning system. *Geophysical Research Letters*, **36**, L00B05.
- [9] Allen RM, Brown H, Hellweg M, Khainovski O, Lombard P, Neuhauser D (2009): Real-time earthquake detection and hazard assessment by ElarmS across California. *Geophysical Research Letters*, **36**, L00B08.
- [10] Allen RM, Gasparini P, Kamigaichi O, Böse M (2009): The status of earthquake early warning around the world: An introductory overview. *Seismological Research Letters*, **80**, 682-693.
- [11] Wurman G, Allen RM, Lombard P (2007): Toward earthquake early warning in northern California. *Journal of Geophysical Research*, **112**, B08311.
- [12] Erdik M, Fahjan Y, Ozel O, Alcik O, Mert A, Gul M (2003): Istanbul earthquake rapid response and early warning system. *Bulletin of Earthquake Engineering*, **1**, 157-163.
- [13] Ionescu C, Böse M, Wenzel F (2007): An early warning system for deep Vrancea (Romania) earthquakes. In *Earthquake Early Warning Systems*, ed. P. Gasparini, G. Manfredi, and J. Zschau, 343-349, Berlin and Heidelberg: Springer.
- [14] Espinosa-Aranda JM, Cuellar A, Garcia A, Ibarrola G, Islas R, Maldonado S, Rodriguez FH (2009): Evolution of the Mexican Seismic Alert System (SASMEX). *Seismological Research Letters*, **80**, 694-706.
- [15] Böse M, Hauksson E, Solanki K, Kanamori H, Heaton TH (2009): Real-time testing of the on-site warning algorithm in southern California and its performance during the July 29 2008  $M_w$  5.4 Chino Hills earthquake. *Geophysical Research Letters*, **36**, L00B03.
- [16] Zollo A, Amoroso O, Lancieri M, Wu YM, Kanamori H (2010): A threshold-based earthquake early warning using dense accelerometer networks. *Geophysical Journal International*, **183**, 963-974.
- [17] Peng HS, Wu ZL, Wu YM, Yu SM, Zhang DN, Huang WH (2011): Developing a prototype earthquake early warning system in the Beijing capital region. *Seismological Research Letters*, **82**, 394-403.
- [18] Satriano C, Elia L, Martino C, Lancieri M, Zollo A, Iannaccone G (2011): PRESTo, the earthquake early warning system for southern Italy: Concepts, capabilities and future perspectives. *Soil Dynamics and Earthquake Engineering*, **31**, 137-153.
- [19] Kuyuk HS, Allen RM, Brown H, Hellweg M, Henson I, Deuhauser D (2014): Designing a network-based earthquake early warning algorithm for California: Elarms-2. *Bulletin of the Seismological Society of America*, **104**, 162-173.
- [20] Hsiao NC, Wu YM, Shin TC, Zhao L, Teng TL (2009): Development of earthquake early warning system in Taiwan. *Geophysical Research Letters*, **36**, L00B02.
- [21] Lin TL, Wu YM (2010): Magnitude determination using strong ground-motion attenuation in earthquake early warning. *Geophysical Research Letters*, **37**, L07304.
- [22] Lin TL, Wu YM, Chen DY (2011): Magnitude estimation using initial P-wave amplitude and its spatial distribution in earthquake early warning in Taiwan. *Geophysical Research Letters*, **38**, L09303.
- [23] Wu YM, Lin TL, Chao WA, Huang HH, Hsiao NC, Chang CH (2011): Faster short-distance earthquake early warning using continued monitoring of filtered vertical displacement: a case study for the 2010 Jiasian, Taiwan, earthquake. *Bulletin of the Seismological Society of America*, **101**, 701-709.
- [24] Holland A (2003): Earthquake data recorded by the MEMS accelerometer. *Seismological Research Letters*, **74**, 20-26.
- [25] Cochran ES, Lawrence JF, Christensen C, Jakka RS (2009): The quake-catcher network: citizen science expanding seismic horizons. *Seismological Research Letters*, **80**, 26-30.
- [26] Wu YM, Chen DY, Lin TL, Hsieh CY, Chin TL, Chang WY, Li WS, Ker SH (2013): A high-density seismic network for earthquake early warning in Taiwan based on low cost sensors. *Seismological Research Letters*, **84**, 1048-1054.
- [27] Peng CY, Zhu XY, Yang JS, Xue B, Chen Y (2013): Development of an integrated onsite earthquake early warning system and test deployment in Zhaotong, China. *Computers & Geosciences*, **56**, 170-177.



- [28] Wu YM, Zhao L (2006): Magnitude estimation using the first three seconds P-wave amplitude in earthquake early warning. *Geophysical Research Letters*, **33**, L16312.
- [29] Wu YM, Kanamori H, Allen R, Hauksson E (2007): Determination of earthquake early warning parameters,  $\tau_c$  and  $P_d$ , for Southern California. *Geophysical Journal International*, **170**, 711-717.
- [30] ANSS Working Group on Instrumentation, Siting, Installation, and Site Metadata of the Advanced National Seismic System Technical Integration Committee (2008): Instrumentation guidelines for the Advanced National Seismic System. *U.S. Geology Survey Open-File Report 2008-1262*, 41 pp.
- [31] MSV6000 variable capacitance accelerometers. [http://www.mtmems.com/en/product\\_view.asp?id=84](http://www.mtmems.com/en/product_view.asp?id=84).
- [32] ADS1281. <http://www.ti.com/lit/ds/symlink/ads1281.pdf>.
- [33] ProASIC3. <http://www.microsemi.com/products/fpga-soc/fpga/proasic3-e#documents>.
- [34] Evans JR, Allen RM, Chung AI, Cochran ES, Guy R, Hellweg M, Lawrence JF (2014): Performances of several low-cost accelerometers. *Seismological Research Letters*, **85**, 147-158.
- [35] Peng CY, Xue B, Yang JS (2015): Timing for an integrated accelerograph EDAS-AS with GPS and NTP. *International Power, Electronics and Materials Engineering Conference (IPEMEC 2015)*, 214-221.
- [36] Sleeman R, van Eck T (1999): Robust automatic P-phase picking: an on-line implementation in the analysis of broadband seismogram recordings. *Physics of the Earth and Planetary Interiors*, **113**, 265-275.
- [37] Zhang HJ, Thurber C, Rowe C (2003): Automatic P-wave arrival detection and picking with multiscale wavelet analysis for single component recordings. *Bulletin of the Seismological Society of America*, **93**, 1904-1912.
- [38] Baer M, Kradolfer U (1987): An automatic phase picker for local and teleseismic events. *Bulletin of the Seismological Society of America*, **77**, 1437-1445.
- [39] Schweitzer J, Fyen J, Mykkeltveit S (2002): Seismic arrays. In: *Bormman, P. (Ed.), IASPEI New Manual of Seismological Observatory Practice*. GeoForschungsZentrum Potsdam, Potsdam, Germany.
- [40] Trnkoczy A (2002): Understanding and parameter setting of STA/LTA trigger algorithm. In: *Bormman, P. (Ed.), IASPEI New Manual of Seismological Observatory Practice*. GeoForschungsZentrum Potsdam, Potsdam, Germany.
- [41] Trnkoczy A, Havskov J, Ottemöller (2002): Seismic networks. In: *Bormman, P. (Ed.), IASPEI New Manual of Seismological Observatory Practice*. GeoForschungsZentrum Potsdam, Potsdam, Germany.
- [42] Holcomb LG (1989): A direct method for calculating instrument noise levels in side-by-side seismometer evaluations. *U.S. Geology Survey Open-File Report 89-214*, 35 pp.
- [43] Sleeman R, van Wettum A, Trampert J (2006): Three-channel correlation analysis: A new technique to measure instrumental noise of digitizers and seismic sensors. *Bulletin of the Seismological Society of America*, **96**, 258-271.
- [44] Evans JR, Followill F, Hutt CR, Kromer RP, Nigbor RL, Ringler AT, Steim JM, Wielandt E (2010): Method for calculating self-noise spectra and operating ranges for seismographic inertial sensors and recorders. *Seismological Research Letters*, **81**, 640-645.
- [45] Evans JR, Followill F, Hutt CR, Kromer RP, Nigbor RL, Ringler AT, Steim JM, Wielandt E (2012): Method for calculating self-noise spectra and operating ranges for seismographic inertial sensors and recorders, Erratum. *Seismological Research Letters*, **83**, 586.
- [46] EpiSensor 2. <http://www.kinematics.com/p-255-Episensor2.aspx>.